

Full-wave-equation depth extrapolation for migration

Kristian Sandberg¹ and Gregory Beylkin²

ABSTRACT

Most of the traditional approaches to migration by downward extrapolation suffer from inaccuracies caused by using one-way propagation, both in the construction of such propagators in a variable background and the suppression of propagating waves generated by, e.g., steep reflectors. We present a new mathematical formulation and an algorithm for downward extrapolation that suppress only the evanescent waves. We show that evanescent wave modes are associated with the positive eigenvalues of the spatial operator and introduce spectral projectors to remove these modes, leaving all propagating modes corresponding to nonpositive eigenvalues intact. This approach suppresses evanescent modes in an arbitrary laterally varying background. If the background velocity is only depth dependent, then the spectral projector may be applied by using the fast Fourier transform and a filter in the Fourier domain. In computing spectral projectors, we use an iteration that avoids the explicit construction of the eigensystem. Moreover, we use a representation of matrices leading to fast matrix-matrix multiplication and, as a result, a fast algorithm necessary for practical implementation of spectral projectors. The overall structure of the migration algorithm is similar to survey sinking with an important distinction of using a new method for downward continuation. Using a blurred version of the true velocity as a background, steep reflectors can be imaged in a 2D slice of the SEG-EAGE model.

INTRODUCTION

Most of the traditional approaches to migration by downward extrapolation use one-way propagators. The reason for that stems from the fact that an initial-value problem with respect to a spatial variable for a second-order hyperbolic equation is ill posed and its solution numerically unstable, as we explain later in the paper. The physical reason for instability is the amplification of evanescent waves that

leads to a rapid blow-up of the solution, making it necessary to suppress unwanted wave modes in downward extrapolation algorithms. In particular, to avoid the blow-up, it is common to construct directional splitting of the propagator.

Examples of migration algorithms that use directional splitting include Stolt migration (Stolt, 1978) and, more generally, downward continuation migrations (see, e.g., Biondi [2006] for an overview). The directional splitting of the propagator carries with it two penalties: the one-directional propagator suppresses not only evanescent waves but also propagating waves moving, for example, in the opposite direction and, in case of variable background, it introduces poorly controlled errors because of the approximation involved in the splitting. For a background with depth-only dependent velocity and zero offset source-receiver configuration, Kosloff and Baysal (1983) propose suppressing only the evanescent waves in the wavenumber domain by using the Fourier transform and a simple ideal cutoff filter. For a general variable background, relying on the Fourier transform as a tool, they suggest using a cutoff filter adjusted to the maximum velocity at a given depth level. As we show in our examples, such strategy leads to the removal of some propagating waves along with the evanescent waves and, as a result, poor imaging of steep reflectors. We note that in the context of ultrasonic imaging, for a constant background, the idea of removing only evanescent waves by the same approach is used by Natterer and Wubbeling (1995, 2005), and Natterer (1997a, 1997b).

To improve downward continuation schemes for laterally variable velocity background, some methods combine the result from multiple migrations using different (constant) reference velocities. The results from these migrations are then combined using some type of interpolation scheme (see e.g. Kessinger [1992] and Biondi [2002, 2006] and references therein for further descriptions of such methods).

In this paper, we propose a mathematical formalism and an algorithm for wavefield extrapolation that allows us to suppress only the evanescent waves for a general variable background, thus yielding what we call full-wave-equation depth extrapolation for migration. The overall structure of our algorithm is similar to the usual survey sinking or source-receiver migration introduced by Claerbout

Manuscript received by the Editor 31 December 2008; revised manuscript received 1 April 2009; published online 15 December 2009.

¹GeoEnergy Inc., Houston, Texas, U.S.A. E-mail: kristian@geoenergycorp.com.

²University of Colorado, Department of Applied Mathematics, Boulder, Colorado, U.S.A., and consultant for GeoEnergy, Inc. E-mail: beylkin@colorado.edu.

© 2009 Society of Exploration Geophysicists. All rights reserved.

(1985) with the important distinction that we use the two-way propagators in our formulation of the problem and suppress only evanescent waves. We provide examples and discuss some implications of our approach later in the paper.

We observe that to suppress only the evanescent waves, it is necessary to use a spectral projector on a subspace spanned by eigenfunctions corresponding to the propagating modes. In fact, in the case of depth-dependent background, a composition of the Fourier transform and the ideal cutoff filter in Kosloff and Baysal (1983) constitutes such a projector.

For a general variable background, by using spectral projectors we arrive at a well-conditioned initial-value problem in the spatial variable. We note that an algorithm for computing spectral projectors does not necessarily involve computing the eigensystem for the propagator, most often a prohibitive proposition. The spectral projector (simply related to the sign function of a matrix) may be computed without generating individual eigenvectors and eigenvalues by using matrix iterations (Kenney and Laub [1995]). Matrix polynomial recursions for computing the sign function are used by Auslander and Tsao (1992). However, the algorithms of this type require matrix-matrix multiplications and, without further development, they are still too expensive for practical applications in problems of wave propagation. Efficient representations of matrices to compute spectral projectors were introduced by Beylkin et al. (1999). For applications in problems of wave propagation, Beylkin and Sandberg (2005) further develop the so-called partitioned low rank (PLR) representation. This representation allows us to reduce the cost of computing spectral projectors. Using the PLR representation, we introduce the full-wave-equation extrapolation for depth migration and demonstrate its performance. Our method makes no assumptions about lateral velocity variations, permitting the recovery of steep reflectors in our examples. Further work is required to make our approach practical in three dimensions and demonstrate its performance with real data, but the very fact that it is possible to suppress only evanescent waves and avoid approximations in splitting the up- and downgoing waves is of importance.

We demonstrate performance of the new migration algorithm on the SEG-EAGE model (Aminzadeh et al., 1996) in two spatial dimensions. We conclude with a discussion on the merits of our approach in relation to other migration methods.

NOTATION

Let us formulate the problem in dimension $d = 3$ using the Cartesian coordinate system (x, y, z) with $z \geq 0$ in the domain of interest. For simplicity, we assume that all sources and receivers are located at the surface in the plane $z = 0$. Let $\mathbf{x}_s = \{(x_i^s, y_i^s)\}_{i=1}^{N_s}$ denote the horizontal coordinates of the sources, $\mathbf{x}_r = \{(x_i^r, y_i^r)\}_{i=1}^{N_r}$ those of the receivers, and (\mathbf{x}, z) a general position in space, where $\mathbf{x} = (x, y)$. We refer to the set of all measurements as a survey which we denote as $u(\mathbf{x}_s, \mathbf{x}_r, z, t)$. A survey consists of $N_s \times N_r$ traces (time series) of measured data and, as usual, we refer to the set of all measurements for a fixed source as a source gather and, to the set of all measurements for a fixed receiver, as a receiver gather. Initially, only the survey at $z = z_0$ is known.

Throughout the paper, we define the Fourier transform and its inverse as

$$\hat{u}(\omega) = \int_{-\infty}^{\infty} u(t) e^{-2\pi i \omega t} dt$$

and

$$u(t) = \int_{-\infty}^{\infty} \hat{u}(\omega) e^{2\pi i \omega t} d\omega.$$

We denote the Fourier transform of all traces in the survey with respect to time as $\hat{u}(\mathbf{x}_s, \mathbf{x}_r, z, \omega)$, where ω denotes time frequency.

PROBLEM FORMULATION

Given a survey $u(\mathbf{x}_s, \mathbf{x}_r, z = z_0, t)$ recorded at a surface, our goal is to find an image of the reflectors that produced the measurement data. We assume that the background velocity model $v(\mathbf{x}, z)$ is available. We also assume that the propagation is described by the acoustic wave equation,

$$\begin{aligned} p_{tt} &= v(\mathbf{x}, z)^2 (p_{xx} + p_{yy} + p_{zz}), \\ p(\mathbf{x}, 0, t) &= 0, \quad t \geq 0, \\ \begin{cases} p(\mathbf{x}, z, 0) = f(\mathbf{x}), \\ p_t(\mathbf{x}, z, 0) = g(\mathbf{x}), \end{cases} \end{aligned} \quad (1)$$

together with absorbing boundary conditions on all boundaries except the surface $z = 0$, where we impose the reflecting condition for $t \geq 0$. Here $v(\mathbf{x}, z)$ is the velocity, $p(\mathbf{x}, z, t)$ is the acoustic pressure at the point (\mathbf{x}, z) , and subscripts indicate partial derivatives. We note that the survey is collected slightly below the surface at $z = z_0$ because at the surface, $z = 0$, the pressure is zero. We note that alternative formulations may involve a source term instead of the initial conditions or a different type of recorded data.

In this paper, we develop a migration method based on the concept of survey sinking, sometimes referred to as source-receiver migration (Claerbout, 1985; Biondi, 2006). The idea is that given a background velocity function $v(\mathbf{x}, z)$ and a survey recorded at the surface $z = z_0$, we compute what the survey would look like at $z_n = z_0 + n\Delta z$, $n = 0, 1, \dots$, where Δz is the desired depth resolution. On taking the Fourier transform, we propagate the survey $\hat{u}(\mathbf{x}_s, \mathbf{x}_r, z_n, \omega)$ for each frequency ω separately. The key to our approach is the new way of downward continuation that yields a stable propagator that suppresses only evanescent waves. By using spectral projectors, we also avoid approximations associated with lateral velocity variations.

We define the migrated image as

$$I(\mathbf{x}, z_n) = \int_{-\infty}^{\infty} \hat{u}(\mathbf{x}_s, \mathbf{x}_r, z_n, \omega) \big|_{\mathbf{x}_s = \mathbf{x}_r = \mathbf{x}} d\omega, \quad n = 0, 1, \dots \quad (2)$$

The integral in equation 2 is also known as the imaging condition and may be interpreted as the inverse Fourier transform with respect to ω of the survey at zero offset, evaluated at zero time ($t = 0$), (Claerbout, 1985; Biondi, 2006; Sava and Hill, 2009). Specifically, to evaluate equation 2, we first extrapolate in depth all source gathers

$\hat{u}(\mathbf{x}_s, \mathbf{x}_r, z_n, \omega)$ to $z_{n+1} = z_n + \Delta z$. We then take the resulting survey and extrapolate in depth all receiver gathers, again by a step Δz . Finally, we interpolate the result to zero offset $\mathbf{x}_s = \mathbf{x}_r$ and sum over all frequencies. Note that we do not compute the cross-correlation of the source and the scattered fields, although these imaging conditions may be equivalent (Biondi, 2006) with their practical efficiency depending on the acquisition geometry (Jeannot, 1988; Biondi and Palacharla, 1996; Biondi, 2006; Sava and Hill, 2009).

In order to begin constructing equations to describe survey sinking, let us apply the Fourier transform with respect to time in equation 1 and consider the result as an equation for \hat{p} ,

$$\hat{p}_{zz} = \left[- \left(\frac{2\pi\omega}{v(\mathbf{x},z)} \right)^2 - D_{xx} - D_{yy} \right] \hat{p} \equiv L\hat{p}. \quad (3)$$

Depending on the conditions at the boundary in the lateral direction (for a fixed depth z), the self-adjoint operator L may have either continuous or discrete spectrum. However, because in either case we use a discrete version of L , we treat it as having a discrete spectrum with real eigenvalues $\{\lambda_k\}_{k=0}^{\infty}$ and a complete set of normalized eigenfunctions $\{e_k(\mathbf{x})\}_{k=0}^{\infty}$ (Grimbergen et al., 1998; Wapenaar and Grimbergen, 1998).

We consider equation 3 with the initial conditions q and q_z at the surface $z = z_n$ (assuming that we already have a survey from the previous depth level)

$$\begin{cases} \hat{p}(\mathbf{x}, z_n, \omega) = q(\mathbf{x}, z_n, \omega) \\ \hat{p}_z(\mathbf{x}, z_n, \omega) = q_z(\mathbf{x}, z_n, \omega) \end{cases}. \quad (4)$$

Formally, we may view equations 3 and 4 as an initial-value problem in z . Unfortunately, such an initial-value problem is ill conditioned and is numerically unstable. Our goal is to construct a well-posed, stable alternative to equations 3 and 4.

ILL-POSEDNESS OF DOWNWARD CONTINUATION

We start by motivating our approach. The cause of instability of the initial-value problem (equations 3 and 4) is the indefinite nature of the self-adjoint operator L , namely, the fact that it has both positive and negative eigenvalues. Negative eigenvalues correspond to propagating modes, and the positive eigenvalues are associated with the nonpropagating evanescent waves and are responsible for the ill-posedness of this initial-value problem.

To illustrate the ill-posedness, let us consider a simple 2D example of downward continuation in a periodic medium with constant velocity v ,

$$\begin{aligned} u_{zz} &= \left(- \frac{4\pi^2\omega^2}{v^2} - D^2 \right) u, \quad x \in (0, 2\pi) \\ u(0, z) &= u(2\pi, z) \\ u(x, 0) &= \sum_{k=-\infty}^{\infty} \alpha_k e^{ikx} \\ u_z(x, 0) &= \sum_{k=-\infty}^{\infty} \beta_k e^{ikx} \end{aligned} \quad (5)$$

The explicit solution of this problem is given by

$$\begin{aligned} u(x, z) &= \frac{1}{2} \sum_{k=-\infty}^{\infty} \left(\alpha_k - \frac{i\beta_k}{k_z} \right) e^{i(kx + k_z z)} \\ &\quad + \left(\alpha_k + \frac{i\beta_k}{k_z} \right) e^{i(kx - k_z z)} \end{aligned} \quad (6)$$

where

$$k_z = \sqrt{\frac{4\pi^2\omega^2}{v^2} - k^2}. \quad (7)$$

Because k_z is imaginary if $k > 2\pi\omega/v$, we observe that some of the modes in equation 6 grow exponentially fast, resulting in a blow-up of the solution. We also note that the eigenvalues in this problem are given by $\lambda_k = -4\pi^2\omega^2/v^2 + k^2$, $k = 0, 1, \dots$ and the eigenvalues corresponding to the unstable modes satisfying $k > 2\pi\omega/v$ are positive.

In Kosloff and Baysal (1983) and later, more systematically, in Natterer and Wubbeling (1995 and 2005) and Natterer (1997a, 1997b), the authors address the stability problem by applying an ideal low-pass filter to remove all modes with $k > 2\pi\omega/v$ after each step, thereby suppressing the evanescent modes. Generalizing this approach to problems with laterally varying background velocity, Kosloff and Baysal (1983) suggest removing all modes $k > 2\pi\omega/\max_x v(x)$ at a given depth. Unfortunately, as we demonstrate in our examples below, using this condition causes unwanted artifacts and poor imaging of steep reflectors. Baysal et al. (1983) introduce the reverse time migration and it appears that the approach in Kosloff and Baysal (1983) has been abandoned. In what follows, we formulate a stable depth extrapolation problem for a general background and demonstrate its advantages.

SPECTRAL PROJECTORS

Let us consider domain A in variable $\mathbf{x} = (x, y)$ representing a receiver or source location. Let L be a self-adjoint operator acting on functions defined on the domain A and having a complete set of normalized eigenfunctions $\{e_k(\mathbf{x})\}_{k=0}^{\infty}$, $\mathbf{x} \in A$. We define the *projector* P_k on the eigenfunction $e_k(\mathbf{x})$ by

$$P_k: f(\mathbf{x}) \mapsto \left(\int_A f(\mathbf{x}') e_k(\mathbf{x}') d\mathbf{x}' \right) e_k(\mathbf{x}),$$

so that the operator L may be written as

$$L = \sum_{k=0}^{\infty} \lambda_k P_k. \quad (8)$$

We define the spectral projector on the nonpositive part of the spectrum as

$$\mathcal{P} = \sum_{\{k: \lambda_k \leq 0\}} P_k, \quad (9)$$

and the propagating part of the operator L as

$$\mathcal{P}L\mathcal{P} = \sum_{\{k: \lambda_k > 0\}} \lambda_k P_k,$$

where, as a result, all eigenvalues of the operator $\mathcal{P}L\mathcal{P}$ are negative or zero. Next, we replace the ill-posed problem (equations 3 and 4) with

$$\begin{aligned} \hat{p}_{zz} &= \mathcal{P}L\mathcal{P}\hat{p}, \\ \left\{ \begin{aligned} \hat{p}(\mathbf{x}, z_n, \omega) &= q(\mathbf{x}, z_n, \omega) \\ \hat{p}_z(\mathbf{x}, z_n, \omega) &= q_z(\mathbf{x}, z_n, \omega) \end{aligned} \right. \end{aligned} \quad (10)$$

thus removing the growing modes causing instability.

The difficulty now shifts to computing the spectral projector \mathcal{P} . Because of the definition of the spectral projector, it may appear necessary to compute the eigensystem of the operator L . However, we use an alternative approach (described in Appendix A) that does not require the direct computation of the eigensystem. Methods for computing spectral projectors or, equivalently, the so-called sign function of a matrix, because $\mathcal{P} = (I - \text{sign}(L))/2$, may be found in the survey [Kenney and Laub \(1995\)](#). Polynomial recursions for this purpose are used by [Auslander and Tsao \(1992\)](#). The main difficulty in using recursions is that they require matrix-matrix multiplications and, thus, may not be practical for large-size problems. The key point of our approach is that we consider matrix representations that remain sparse (up to finite but arbitrary accuracy) throughout the iteration that produces the spectral projector. Such approach first appears in [Beylkin et al. \(1999\)](#) using sparse representations for a class of operators of interest in quantum chemistry. For problems of wave propagation, the so-called partitioned low rank (PLR) representation is further developed and used by [Beylkin and Sandberg \(2005\)](#). Using PLR representation of matrices allows us to obtain a reasonable speed for computing spectral projectors (see Appendix A for further details).

SOURCE/RECEIVER DOWNWARD CONTINUATION

In order to compute the survey at z_{n+1} , we recursively downward continue the survey from z_n to z_{n+1} based on solving equation 10 in the frequency domain.

In the first step, we downward continue all source gathers from z_n to z_{n+1} , resulting in a new survey, which we denote as $\tilde{u}(\mathbf{x}_s, \mathbf{x}_r, z_n, \omega)$. This intermediate survey models what the survey would look like if all sources were located at z_n and all receivers were located at z_{n+1} .

The intermediate survey \tilde{u} is computed by solving

$$\begin{aligned} \hat{p}_{zz} &= \mathcal{P}L\mathcal{P}\hat{p}, \\ \left\{ \begin{aligned} \hat{p}(\mathbf{x}, z_n, \omega) &= \hat{u}(\mathbf{x}_s, \mathbf{x}_r, z_n, \omega) \\ \hat{p}_z(\mathbf{x}, z_n, \omega) &= \hat{u}_z(\mathbf{x}_s, \mathbf{x}_r, z_n, \omega) \end{aligned} \right. \end{aligned} \quad (11)$$

for each source gather i . In other words, solving equation 11 maps the source gather $\hat{u}(\mathbf{x}_s, \mathbf{x}_r, z_n, \omega)$ to the downward continued source gather $\tilde{u}(\mathbf{x}_s, \mathbf{x}_r, z_n, \omega)$.

In the second step, we downward continue all receiver gathers of $\tilde{u}(\mathbf{x}_s, \mathbf{x}_r, z_n, \omega)$ from z_n to z_{n+1} . The resulting survey $\hat{u}(\mathbf{x}_s, \mathbf{x}_r, z_{n+1}, \omega)$ models what the survey would look like if all sources and receivers were located at $z = z_{n+1}$.

The downward continued survey \hat{u} is computed by solving

$$\begin{aligned} \hat{p}_{zz} &= \mathcal{P}L\mathcal{P}\hat{p}, \\ \left\{ \begin{aligned} \hat{p}(\mathbf{x}, z_n, \omega) &= \tilde{u}(\mathbf{x}_s, \mathbf{x}_r, z_n, \omega) \\ \hat{p}_z(\mathbf{x}, z_n, \omega) &= \tilde{u}_z(\mathbf{x}_s, \mathbf{x}_r, z_n, \omega) \end{aligned} \right. \end{aligned} \quad (12)$$

for each receiver gather j . In other words, solving equation 12 maps

the receiver gather $\tilde{u}(\mathbf{x}_s, \mathbf{x}_r, z_n, \omega)$ to the downward continued receiver gather $\hat{u}(\mathbf{x}_s, \mathbf{x}_r, z_{n+1}, \omega)$.

In order to initialize the iteration, we need the normal derivative of the wavefield at the surface $\hat{u}_z(\mathbf{x}_s, \mathbf{x}_r, z = z_0, \omega)$ which typically is not available from the field data. However, assuming constant-velocity background near the surface, we can estimate $\hat{u}_z(\mathbf{x}_s, \mathbf{x}_r, z = z_0, \omega)$ from $\hat{u}(\mathbf{x}_s, \mathbf{x}_r, z = z_0, \omega)$ using the same approach as in [Kosloff and Baysal \(1983\)](#). In two dimensions, we compute the normal derivative from $\hat{u}(x, z = z_0, \omega)$ as

$$\begin{aligned} \hat{u}_z(x, z = z_0, \omega) &= \int_{-2\pi/\omega}^{2\pi/\omega} \left(i \sqrt{\frac{4\pi^2\omega^2}{v^2} - k^2} \right. \\ &\quad \left. \times \int_{-\infty}^{\infty} \hat{u}(x, z = z_0, \omega) e^{-2\pi i k x} dx \right) e^{2\pi i k z} dk, \end{aligned} \quad (13)$$

where integrals are evaluated using the fast Fourier transform (FFT). The assumption of a constant velocity near the surface also allows us to use an ideal low-pass filter in the spatial wavenumber domain to suppress evanescent waves at this initial step of the algorithm.

ALGORITHM

Let us describe the steps of our migration algorithm. We define the forward operator L as in equation 3 and the projector \mathcal{P} as in equation 9. We write the downward continuation problem $\hat{p}_{zz} = \mathcal{P}L\mathcal{P}\hat{p}$ as the first-order system

$$\frac{d}{dz} \begin{bmatrix} \hat{p} \\ \hat{p}_z \end{bmatrix} = \begin{bmatrix} 0 & 1 \\ \mathcal{P}L\mathcal{P} & 0 \end{bmatrix} \begin{bmatrix} \hat{p} \\ \hat{p}_z \end{bmatrix} \quad (14)$$

together with initial conditions given by the source or receiver gathers from the previous depth level.

Our algorithm may now be formulated as follows:

1. Initialize the migrated image $I = 0$.
2. **for** all frequencies $\omega_m, m = 1, \dots, M$:
 - for** all depth steps $n = 1, \dots, N$:
 - (a) **for** all sources $i = 1, \dots, N_s$:
 - i. Compute the spectral projector \mathcal{P} (see Appendix A).
 - ii. Downward continue $\hat{u}(\mathbf{x}_s, \mathbf{x}_r, z_n, \omega)$ and $\hat{u}_z(\mathbf{x}_s, \mathbf{x}_r, z_n, \omega)$ to $\tilde{u}(\mathbf{x}_s, \mathbf{x}_r, z_n, \omega)$ and $\tilde{u}_z(\mathbf{x}_s, \mathbf{x}_r, z_n, \omega)$, respectively, by solving equation 14 with $\hat{u}(\mathbf{x}_s, \mathbf{x}_r, z_n, \omega)$ and $\hat{u}_z(\mathbf{x}_s, \mathbf{x}_r, z_n, \omega)$ as the initial condition.
 - (b) **for** all receivers $j = 1, \dots, N_r$:
 - i. Compute the spectral projector \mathcal{P} (see Appendix).
 - ii. Downward continue $\tilde{u}(\mathbf{x}_s, \mathbf{x}_r, z_n, \omega)$ and $\tilde{u}_z(\mathbf{x}_s, \mathbf{x}_r, z_n, \omega)$ to $\hat{u}(\mathbf{x}_s, \mathbf{x}_r, z_{n+1}, \omega)$ and $\hat{u}_z(\mathbf{x}_s, \mathbf{x}_r, z_{n+1}, \omega)$, respectively, by solving equation 14 with $\tilde{u}(\mathbf{x}_s, \mathbf{x}_r, z_n, \omega)$ and $\tilde{u}_z(\mathbf{x}_s, \mathbf{x}_r, z_n, \omega)$ as the initial condition.
 - (c) Interpolate the survey $\hat{u}(\mathbf{x}_s, \mathbf{x}_r, z_{n+1}, \omega)$ to zero offset $\hat{u}(\mathbf{x}_s = \mathbf{x}, \mathbf{x}_r = \mathbf{x}, z_{n+1}, \omega)$

- (d) Update the migrated image $I(\mathbf{x}, z_{n+1}) = I(\mathbf{x}, z_n) + \hat{u}(\mathbf{x}_s = \mathbf{x}, \mathbf{x}_r = \mathbf{x}, z_{n+1}, \omega)$

For propagating the wavefield from z_n to z_{n+1} , we use an algorithm based on Coult et al. (2006) that has practically insignificant numerical dispersion. We note that in some cases the source-receiver configuration may allow the same spectral projector to be used for downward continuing several gathers. For example, if the source and receiver grids coincide, so do the corresponding projectors.

We also note that if the velocity varies only in depth but not horizontally, then applying the spectral projector to the operator is equivalent to applying an ideal low-pass filter in the spatial wavenumber domain. In such situations, our method is similar to the method proposed in Kosloff and Baysal (1983), as noted earlier in the discussion of ill-posedness of downward continuation.

We implement the absorbing boundary conditions using a variant of the approach of Cerjan et al. (1985). This allows us to decouple the application of the absorbing boundary conditions from the application of spectral projectors. As a result, we need to compute the spectral projector in a slightly extended domain but only for either periodic or zero boundary condition. As a result, the operator on the extended domain remains self-adjoint so that we may use the algorithm in Appendix A.

Computing costs

We estimate the computing costs of 3D survey sinking except for the cost of computing spectral projectors which we estimate only in two dimensions. Computing spectral projectors in three dimensions is part of further research, and we expect significant savings by developing fast algorithms for this purpose. Let N_{hx} and N_{hy} denote the number of offsets in the survey, N_z the number of depth steps, N_f the number of frequencies, and $N_x(\omega_k)$, $N_y(\omega_k)$ describe the size of the computational grid in the horizontal plane for a given frequency ω_k .

The total computational cost for wide-azimuth survey sinking in three dimensions may be estimated as

$$C_{\text{total}} = \sum_{k=1}^{N_f} N_{hx} N_{hy} N_z C_{\text{DE}}(N_x(\omega_k), N_y(\omega_k)).$$

Here C_{DE} denotes the cost of extrapolating the survey one depth step. The cost depends on the size of computational grid. We note that we may choose lower sampling rates for lower frequencies, i.e., use an adaptive approach.

For a given frequency ω_k , the cost C_{DE} may be broken up as

$$C_{\text{DE}} = C_{\text{WE}}(N_x, N_y) + C_{\text{proj}}(N_x, N_y)$$

where C_{WE} denotes the cost of extrapolating one depth step in equation 14 and C_{proj} the cost of computing the projector \mathcal{P} . The cost C_{WE} depends on the solver for equation 14. For example, for a finite difference scheme $C_{\text{WE}} = O(N_x N_y)$, whereas for a spectral scheme $C_{\text{WE}} = O(N_x \log(N_x) N_y \log(N_y))$. In our current implementation the cost of computing the projector in two dimensions is $C_{\text{proj}} = O(N_x \log(N_x)^2)$.

Impulse response

As a way of comparing with other approaches to downward extrapolation, we provide the impulse response of our method in a constant background. This by itself does not describe the quality of an

imaging algorithm in a variable background, but it gives a quick way to assess some of its properties.

We compute the impulse response of the depth extrapolation scheme defined by equation 14. Considering a domain of 2000 m deep and 4000 m wide with constant velocity of 1500 m/s, we position the point source at $x = 2000$ and $z = 0$ and record its field $p(x_i, z = 0, t)$ at an equally spaced receiver array $x_i = 10i$, $i = 0, \dots, 400$ using a Ricker wavelet with dominating frequency at 7 Hz. We then compute $\hat{p}(x_i, z = 0, \omega)$ and apply our downward extrapolation in depth to obtain $\hat{p}(x_i, z, \omega)$. Using the imaging condition at time $t = 1$,

$$I(x, z) = \int_{-\infty}^{\infty} \hat{p}(x_i, z, \omega) e^{2\pi i \omega} d\omega,$$

we display the result in Figure 1. The impulse response indicates excellent performance for all angles.

RESULTS AND DISCUSSION

Our goal in this section is to demonstrate the performance of our method on a synthetic example. As a background velocity, we use two smoothed versions of the true velocity, one moderately (example 1) and another heavily blurred (example 2). We compare our approach to that of using a combination of the Fourier transform and the ideal cutoff filter adjusted to the maximum velocity at each depth level in order to make downward depth propagation stable as suggested by Kosloff and Baysal (1983). The latter is a natural (but, as it turns out, rather inaccurate) approximation as it suppresses waves necessary for proper image formation, for example, of steep reflectors. We find it instructive to compare the effect of such approximation to the result of our approach. The moderately blurred background velocity of example 1 (see below) is fairly close to the true velocity and, in this case, our migration produces an image that includes steep reflectors and practically no artifacts inside the simulated salt dome.

We do not compare our results with those obtained by other migration methods and, instead, rely on the fact that we use a model for which such results are available in the literature (e.g., Stoffa et al., 2006).

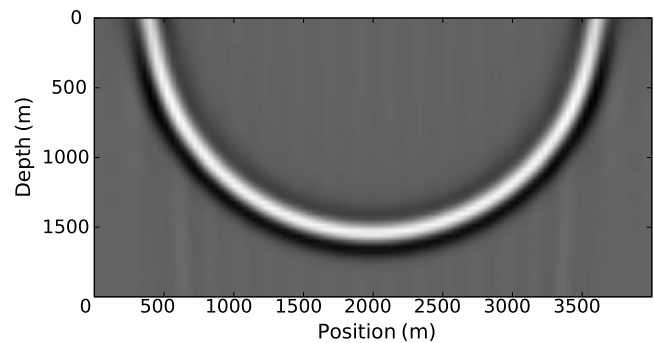


Figure 1. Impulse response from a point source at $x = 2000$ and $z = 0$ using a Ricker source wavelet with a dominating frequency of 7 Hz.

Generating the survey

We generate data for our experiments using slice 337 in the crossline dimension of the SEG-EAGE model (Figure 2a). The same slice was used by Stoffa et al. (2006). The input model has the physical dimension $13,500 \times 4000$ m.

The receiver data was generated by using the modeling algorithm described by Coult et al. (2006) with absorbing boundary conditions at the sides. We used a Ricker pulse with a dominating frequency of 7 Hz, and recorded a 12 s time trace for each shot. We placed sources

at shot locations $x_i^s = i\Delta x$, $i = 0, \dots, 675$ where $\Delta x = 20$ m. For each source i , we placed receivers at $x_{j,i}^r = x_i^s + j\Delta x$, $j = -68, \dots, 68$. Hence, the receiver aperture for each shot corresponds to 2700 m, or one-fifth of the lateral extent of the domain, except for sources near the boundaries where the receiver array was truncated in order to fall within the modeling domain.

Example 1

As background velocity for the migration algorithm, we used a blurred version of the original velocity model in Figure 2a. The velocity model was generated by first applying a median filter using a 3×3 mask, followed by applying a 5×5 averaging mask, where each element in the mask was set to $1/25$. The purpose of the median filter is to (completely) remove the line-like reflectors in the original model, whereas the averaging mask blurs the interfaces. The resulting blurred model is shown in Figure 2b.

We first used the ideal low-pass filter in the spatial wavenumber domain, as described by Kosloff and Baysal (1983). The migrated image is shown Figure 3a. We note that most of the reflectors above the salt body are accurately imaged as well as the top and the bottom of the salt body. However, steep structures such as the left flank of the salt body are not imaged correctly.

Next, we used spectral projectors as described in the Algorithm section. The result is shown in Figure 3b. Comparing Figure 3a and b, we note a significant improvement in imaging of steep structures. Despite the relative narrow aperture of the receiver array, the salt flank is very well imaged.

Example 2

For our next experiment, we used a heavily blurred version of the background velocity. The velocity model was generated by first applying a median filter using a 3×3 mask, followed by applying a 25×25 averaging mask where each element in the mask was set to $1/625$. The resulting blurred model is shown in Figure 2c.

We first used the ideal low-pass filter in the spatial wavenumber domain as described by Kosloff and Baysal (1983). The migrated image is shown in Figure 4a. Next, we used spectral projectors as de-

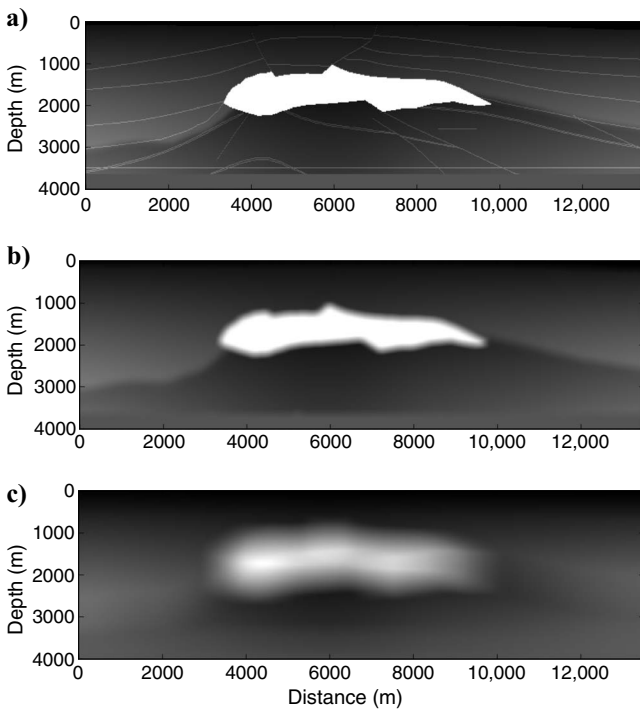


Figure 2. (a) Original velocity model and two background velocities used for migration in (b) example 1 and (c) example 2, obtained by blurring the original model.

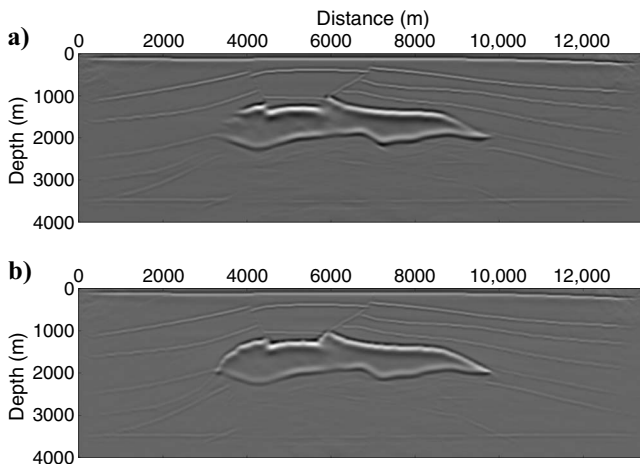


Figure 3. Comparison of migrated images using the moderately blurred background velocity of Example 1. Results of using (a) the ideal low-pass filter and (b) spectral projectors. Migration using spectral projectors recovers steep reflectors and is nearly free from artifacts inside the salt dome.

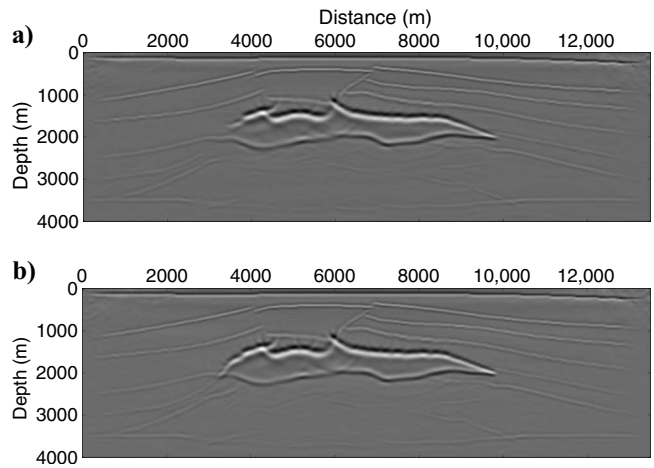


Figure 4. Comparison of migrated images using the heavily blurred background velocity of Example 2. Results of using (a) the ideal low-pass filter and (b) spectral projectors. Despite a relatively poor background velocity model, migration using spectral projectors still recovers steep reflectors.

scribed in the Algorithm section. The result is shown in Figure 4b.

Comparing Figure 4a and b, we note that the shape of the salt body is remarkably well preserved despite the inexact velocity model. We also note that although the velocity model in Figure 2c does not contain significant velocity variations, the spectral projector method still gives a significant advantage over the method using an ideal low-pass filter.

CONCLUSION

Migration schemes based on factorization of operator L in equation 3 into up- and downgoing waves produce errors because of suppression of propagating waves and, in a variable background, because of approximate factorization of the operator. Alternative approaches in variable background that exist today are two-way equation schemes based on using the initial-value problem in time. Such reverse-time migration schemes change the inverse problem so that “local interactions” between events are now in time rather than in depth. A careful comparison of our full-wave-equation depth extrapolation for migration with that of reverse-time migration is beyond the topic of this paper and should be a subject of further research.

Our formulation of the downward-continuation operator removes only nonpropagating evanescent waves, thus preserving propagating waves moving in all directions. We have demonstrated significant improvement in imaging by comparing our approach to that of a method where most but not all propagating waves are preserved, hence emphasizing the sensitivity of imaging to the erroneous removal of propagating waves.

While our method is computationally more expensive than some simpler techniques, the quality of the results justifies the effort to develop fast 3D algorithms for this type of migration and inversion. We plan to develop our approach further to a full 3D version and work on making our algorithm competitive with other migration methods in terms of speed. We also plan to test full-wave-equation depth extrapolation on real data. Looking beyond these remaining issues, the results of this paper indicate many new interesting possibilities to advance seismic methods, such as to include multiple reflections into image formation and to improve the velocity analysis.

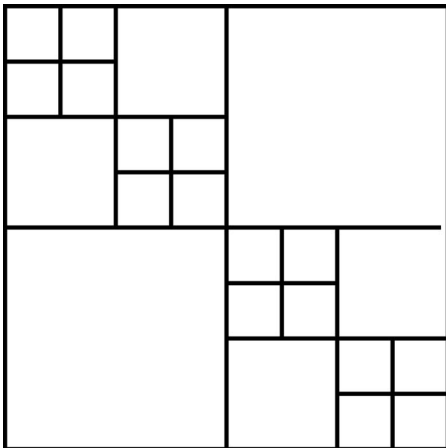


Figure A-1. Matrix partitioning in PLR representation.

ACKNOWLEDGMENTS

This research was supported by GeoEnergy, Inc. The authors would like to thank Anthony Vassiliou for his valuable comments on this paper. We also want to thank the anonymous reviewers for their important comments and suggestions.

APPENDIX A

COMPUTING SPECTRAL PROJECTORS

To compute the spectral projector on the negative part of the spectrum in equation 9, we use a simple iteration scheme (see e.g., Kenney and Laub, 1995; Auslander and Tsao, 1992; and Beylkin et al., 1999).

For a self-adjoint matrix L , the spectral projector \mathcal{P} is simply related to the sign function of a matrix, namely $\mathcal{P} = (I - \text{sign}(L))/2$. In order to find $\text{sign}(L)$, we iterate according to

1. Initialize $\mathcal{S}_0 = L/\|L\|_2$.
2. **For** $k = 1, \dots, N_{it}$:

$$\mathcal{S}_{k+1} = \frac{3}{2}\mathcal{S}_k - \frac{1}{2}\mathcal{S}_k^3.$$

The iteration converges quadratically, $\mathcal{S}_k \rightarrow \text{sign}(L)$. For details on analysis of this iteration, see Beylkin et al. (1999), although the basic proof is simple. Noting that all matrices \mathcal{S}_k are diagonalizable by the same transform, this iteration needs to be verified only in the scalar case. Viewed as a fixed-point iteration, the scalar version has only three fixed points, 1, -1 and 0, where only the first two are stable. We note that the normalization assures that the absolute value of all eigenvalues of \mathcal{S}_0 is less than one, so it is perfectly fine to start with $\mathcal{S}_0 = L/\|L\|_2$ or use any other norm.

In Figure A-1, we illustrate the PLR representation by showing the partitioning of a matrix. In each off-diagonal block, we use a low-rank representation of the individual off-diagonal submatrices as

$$\sum_{k=1}^r \mathbf{u}_k \mathbf{v}_k^T, \quad (15)$$

where \mathbf{u}_k and \mathbf{v}_k , $k = 1, \dots, r$ are vectors of appropriate size for a given block. In this representation, the number of terms r (the rank of an off-diagonal submatrix) is selected for a given user-supplied accuracy and can be found by the singular value decomposition (SVD). However, we note that because we do not require orthogonality between vectors, a simpler algorithm based on the Gram-Schmidt orthogonalization is also available. If the ranks of off-diagonal blocks are small and do not grow with iteration, the cost of multiplying matrices in the PLR representation is $O(M(\log M)^2)$. The operation count depends on the rank, r , but because we rely on it staying small, we treat its impact as a constant factor. For details, see Beylkin and Sandberg (2005).

REFERENCES

- Aminzadeh, F., N. Burkhard, J. Long, T. Kunz, and P. Duclos, 1996, Three-dimensional SEG/EAGE models — An update: The Leading Edge, **15**, 131–134.
- Auslander, L., and A. Tsao, 1992, On parallelizable eigensolvers: Advances in Applied Mathematics, **13**, 253–261.
- Baysal, E., D. D. Kosloff, and J. W. C. Sherwood, 1983, Reverse time migration: Geophysics, **48**, 1514–1524.
- Beylkin, G., N. Coult, and M. J. Mohlenkamp, 1999, Fast spectral projection

- algorithms for density-matrix computations: *Journal of Computational Physics*, **152**, 32–54.
- Beylkin, G., and K. Sandberg, 2005, Wave propagation using bases for band-limited functions: *Wave Motion*, **41**, 263–291.
- Biondi, B., 2002, Stable wide-angle Fourier finite-difference downward extrapolation of 3D wavefields: *Geophysics*, **67**, 872–882.
- , 2006, 3D seismic imaging: SEG.
- Biondi, B., and G. Palacharla, 1996, 3-D prestack migration of common-azimuth data: *Geophysics*, **61**, 1822–1832.
- Cerjan, C., D. Kosloff, R. Kosloff, and M. Reshef, 1985, A nonreflecting boundary condition for discrete acoustic and elastic wave equation: *Geophysics*, **50**, 705–708.
- Claerbout, J. F., 1985, *Imaging the earth's interior*: Blackwell Scientific Publications, Inc.
- Coult, N., K. Sandberg, G. Beylkin, and A. Vassiliou, 2006, Acoustic and elastic modeling using bases for bandlimited functions: 76th Annual International Meeting, SEG, Expanded Abstracts, 2241–2244.
- Grimbergen, J., F. Dessing, and K. Wapenaar, 1998, Modal expansion of one-way operators in laterally varying media: *Geophysics*, **63**, 995–1005.
- Jeannot, J., 1988, Full prestack versus shot record migration: Practical aspects: 58th Annual International Meeting, SEG, Expanded Abstracts, 966–968.
- Kenney, C., and A. Laub, 1995, The matrix sign function: *IEEE Transactions on Automatic Control*, **40**, 1330–1348.
- Kessinger, W., 1992, Extended split-step Fourier migration: 62nd Annual International Meeting, SEG, Expanded Abstracts, 917–920.
- Kosloff, D., and E. Baysal, 1983, Migration with the full acoustic equation: *Geophysics*, **48**, 677–687.
- Natterer, F., 1997a, An algorithm for 3D ultrasound tomography, in G. Chavent and P. C. Sabatier, eds., *Inverse problems of wave propagation and diffraction*: Springer, 216–225.
- , 1997b, An initial value approach to the inverse Helmholtz problem at fixed frequency, in H. W. Engl, A. K. Louis, and W. Rundell, eds., *Inverse problems in medical imaging and nondestructive testing*: Springer, 159–167.
- Natterer, F., and F. Wubbeling, 1995, A propagation-backpropagation method for ultrasound tomography: *Inverse Problems*, **11**, 1225–1232.
- , 2005, Marching schemes for inverse acoustic scattering problems: *Numerische Mathematik*, **100**, 697–710.
- Sava, P., and S. Hill, 2009, Overview and classification of wavefield seismic imaging methods: *The Leading Edge*, **28**, 170–183.
- Stoffa, P. L., M. K. Sen, R. K. Seifoullaev, R. C. Pestana, and J. T. Fokkema, 2006, Plane-wave depth migration: *Geophysics*, **71**, no. 6, S261–S272.
- Stolt, R. H., 1978, Migration by Fourier transform: *Geophysics*, **43**, 23–48.
- Wapenaar, K., and J. Grimbergen, 1998, A discussion on stability analysis of wave field depth extrapolation: 68th Annual International Meeting, SEG, Expanded Abstracts, 1716–1719.